polysaccharides

MDPI

Article

Early Chondrogenic Differentiation of Spheroids for Cartilage Regeneration: Investigation of the Structural and Biological Role of a Lactose-Modified Chitosan

Marco Conz [1], Francesca Scognamiglio [1,*], Ivan Donati [1], Susi Zara [2], Gabriella Teti [3], Maurizio Romano [4] and Eleonora Marsich [5]

[1] Department of Life Sciences, University of Trieste, Via Licio Giorgieri 5, 34127 Trieste, Italy; marco.conz@studenti.units.it (M.C.); idonati@units.it (I.D.)
[2] Department of Pharmacy, University "G. d'Annunzio" Chieti-Pescara, Via dei Vestini 31, 66100 Chieti, Italy; s.zara@unich.it
[3] Department of Biomedical and Neuromotor Sciences, University of Bologna, Via Irnerio 48, 40126 Bologna, Italy; gabriella.teti2@unibo.it
[4] Department of Life Sciences, University of Trieste, Via Alfonso Valerio 28, 34127 Trieste, Italy; mromano@units.it
[5] Department of Medicine, Surgery and Health Sciences, University of Trieste, Piazza dell'Ospitale 1, 34129 Trieste, Italy; emarsich@units.it
* Correspondence: fscognamiglio@units.it

Abstract: Long-term solutions for cartilage repair after injury are currently being investigated, with most research aiming to exploit the regenerative and chondrogenic differentiation potential of stem-cell-based spheroids. The incorporation of the bioactive polymer CTL, a lactose-modified chitosan, into spheroids is a strategy to improve cell viability and accelerate type II collagen gene expression. In this work, the role of CTL in influencing the dynamics of spheroid formation and its interplay with cell membrane adhesion molecules (integrins and cadherins) and cytoskeletal components is elucidated. The results indicate that CTL is actively involved in the reorganization of cells into spheroids. An analysis of the effects of physical form of CTL (rehydrated polymer coating or polymer solution) in stimulating peculiar biological responses indicates that CTL matrix in spheroids facilitates an early phase of chondrogenic differentiation. Once the CTL matrix is included in spheroids, there is an increase in COL2A1 gene expression and matrix deposition, regardless of the initial physical form of CTL. Overall, these results contribute to a better understanding of the dynamics of spheroid formation in the presence of the polymer and on its bioactive role in mesenchymal stem cell spheroids.

Keywords: spheroids; polysaccharides; chondrogenesis; cartilage; collagen; cell adhesion molecules

Academic Editor: Karin Stana Kleinschek

Received: 18 March 2025
Revised: 16 May 2025
Accepted: 29 May 2025
Published: 3 June 2025

Citation: Conz, M.; Scognamiglio, F.; Donati, I.; Zara, S.; Teti, G.; Romano, M.; Marsich, E. Early Chondrogenic Differentiation of Spheroids for Cartilage Regeneration: Investigation of the Structural and Biological Role of a Lactose-Modified Chitosan. *Polysaccharides* **2025**, *6*, 47. https://doi.org/10.3390/polysaccharides6020047

1. Introduction

The regeneration of damaged articular cartilage poses some challenges due to the limited ability of this tissue to self-repair. These limitations are primarily due to the absence of blood and lymphatic vessels and the deposition of type I collagen following an injury, resulting in the formation of fibrous tissue and a loss of the functional and mechanical properties of hyaline cartilage [1,2]. Three-dimensional cell structures such as spheroids have been proposed for the tissue engineering of cartilage, providing several advantages over surgical approaches and strategies based on the use of scaffold materials and 2D cell culture. In monolayer cell cultures, cells display reduced cell–cell and cell–extracellular

matrix (ECM) interactions, which leads to biological responses different from those occurring in vivo, reducing the overall therapeutic efficacy. In spheroids, these interactions are established through the contribution of membrane integrins and cadherins [3–5], so that both the environment and the biological responses achieved in vivo are reproduced with greater similarity than 2D cell cultures [6,7]. Different methods can be employed for spheroid formation, and they can be prepared as cellular aggregates consisting only of cells or as hybrid cell–polymer structures. Polymeric matrices endowed in spheroids can mimic the ECM, providing structural and biological support for spheroid formation, survival, and differentiation. The incorporation of external matrices into spheroids offers advantages in terms of improving the viability and differentiation capability by reducing spheroid compactness and favoring the diffusion of nutrients and differentiation factors [8,9].

Recently, the use of a lactose-modified chitosan (CTL) has been reported for the preparation of biomaterials [10,11], hydrogels for stem cell differentiation [12], and cell–polymer spheroids [13]. These spheroids were prepared by seeding human mesenchymal stem cells (MSCs) onto polymer-coated cell culture wells [13]. Indeed, layers of CTL polymer prevent cell adhesion and induce the formation of cell–cell interactions, which results in the formation of cellular aggregates. The inclusion of CTL in MSC-based spheroids increases spheroid viability and accelerates the synthesis and deposition of type II collagen. These aspects provide some fundamental advantages for an application of these structures in vivo, and allow the early implantation of more viable and differentiated structures [13].

In this work, the dynamics of spheroid formation in the presence of CTL was investigated, and the complex interplay between the polysaccharide, cytoskeleton, and cell–cell and cell–matrix adhesion molecules were elucidated. Cell–polymer spheroids were formed by means of a CTL dry coating and a CTL solution, and the influence of the physical form of the polymer in accelerating the synthesis of COL-2 was analyzed and compared to spheroids devoid of matrices (matrix-free spheroids—MF-spheroids). These results highlight the role of CTL in facilitating cell reorganization into spheroids through cell–polymer interactions and in influencing early chondrogenic differentiation.

2. Materials and Methods

2.1. Materials

Lactose-modified chitosan in hydrochloride form, CTL (CAS Registry Number 85941-43-1), with fractions of N-acetyl-glucosamine (GlcNAc; "acetylated", A) (F_A) = 0.16; glucosamine ($GlcNH_2$; "deacetylated", D) (F_D) = 0.21; and lactitol substituted D unit (N-alkylated GlcLac; "lactitol", L) (F_L) = 0.63, was kindly provided by Biopolife S.r.L. (Trieste, Italy). Agar was kindly provided by Java Biocolloid Europe S.r.L. PBS tablets, Triton X-100, sodium hydroxide (NaOH), formaldehyde 40% *w*/*v*, bovine serum albumin (BSA), Mowiol 4-88, normal goat serum (NGS), TRI-reagent, Fluorescein isothiocyanate (FITC), human mesenchymal stem cells (hMSCs), transforming growth factor-β1 (TGF-β1), dexamethasone, integrin β1-blocking monoclonal antibody (MAB1959), integrin β3-blocking monoclonal antibody (MAB2023Z), E-cadherin-blocking monoclonal antibody (MABT26), paclitaxel, and nocodazole were purchased from Merck. Cytochalasin-D, ML-7 dihydrochloride, Y-27632 dihydrochloride, anti-integrin β1 (SC-9970) mouse antibody, and CruzFluor™ 647-conjugated mouse IgGκ light chain binding protein (sc-516179) were obtained from Santa Cruz Biotechnology. L-ascorbic acid was obtained from Fluka Biochemika. Mesenchymal Stem Cell Growth Medium 2 (MSC medium) was obtained from PromoCell. Fetal bovine serum (FBS), penicillin/streptomycin (P/S), and trypsin–ethylenediaminetetraacetic acid (EDTA) were purchased from EuroClone S.p.A. Insulin–transferrin–selenium–sodium pyruvate (ITS-A 100X), DAPI, goat anti-rat secondary antibody Alexa Fluor™ 568 (A-11077), and M-MLV reverse transcriptase were obtained from

Thermo Fisher Scientific. Hematoxylin, eosin, and Masson trichrome kits for staining, paraffin, balsam, slides, and microtome blades were purchased from Bio-Optica (Milan, Italy). Glutaraldehyde 25% *v*/*v* aqueous solution, cacodylic acid, osmium tetroxide, and epoxy resin were purchased from Merck. FITC was above 90% purity (HPLC), and all other materials were of molecular biology or ACS grade (above 98%).

2.2. Preparation of CTLc-Spheroids, MF-Spheroids, and CTLs-Spheroids

Spheroids cultured on CTL coating (CTLc-spheroids) were prepared according to [13,14]. Briefly, the wells of 24-well cell culture plates were coated with 400 µL of CTL solution (2% *w*/*v* in PBS, pH 7.4) followed by overnight air-drying and UV sterilization. hMSCs derived from adipose tissue were cultured in complete medium (MSC medium, penicillin/streptomycin 1%, supplementary mix 10%). On the day of seeding, 60,000 cells were plated in each well, in 1.5 mL of chondrogenic medium (complete MSC medium supplemented with ascorbic acid 100 µM, dexamethasone 0.1 µM, TGF-β1 10 ng/mL, ITS-A 1×). To prepare matrix-free spheroids (MF-spheroids), the wells of the cell culture plate (24-well) were coated with agar gel (2% *w*/*v* in PBS) and MSCs were seeded in chondrogenic medium at the same cell density (60,000 cells/1.5 mL of medium in each well) as the CTLc-spheroids. Spheroids cultured in the presence of CTL in solution (CTLs-spheroids) were prepared by dissolving the polymer (final concentration = 0.53% *w*/*v*) in chondrogenic medium. Finally, the cells were added to the CTL-containing medium and 1 mL of this solution was seeded on agar-coated wells (60,000 cells/well).

2.3. Spheroid Formation in the Presence of Blocking Antibodies and Cytoskeletal Inhibitory Compounds

CTLc-spheroids and MF-spheroids were prepared as described in Section 2.2, in the presence of the different compounds at the following concentrations: Cytochalasin-D 2 µM, ML-7 hydrochloride 25 µM, Y-27632 hydrochloride 10 µM, nocodazole 10 µM, paclitaxel 10 µM, E-cadherin-blocking antibody (10 µg/mL), and a mixture of integrin-β1-blocking antibody and integrin-β3-blocking antibody (10 µg/mL each). The concentration of each compound was selected according to previous research studies [15].

2.4. Analysis of Spheroid Dimensions

Optical images of spheroids were acquired by an optical microscope (Optech IB3 ICS) equipped with a Pentax K100D camera (Pentax Corporation, Tokyo, Japan), using 4× objective. The analysis of spheroid dimensions was performed using Fiji–ImageJ software (version 2.14.0). For each time point, the area of the spheroids was calculated using the range selection tools and the ROI manager. Data were averaged and standard deviation was calculated. Statistical significance was calculated by unpaired *t*-test analysis.

2.5. Synthesis of CTL Labeled with Fluorescein Isothiocyanate (FITC)

CTL powder (300 mg) was dissolved in deionized water (100 mL) and the FITC solution (1.1 mL; 0.5 mg/mL in sodium bicarbonate buffer 50 mM) was added. Incubation was carried out for 24 h in the dark at room temperature (RT). The solution was then dialyzed (Spectrapore, MWCO 12′000) against $NaHCO_3$ 50 mM, NaCl 100 mM, and, finally, in deionized water until the conductivity was lower than 3 µS/cm at 4 °C. The pH of the solutions was set at 4.5 before freeze-drying using an ALPHA 1−2 LD plus freeze-dryer (CHRIST, Osterode am Harz, Germany).

2.6. Localization of Labeled Polymer in CTLc-Spheroids and CTLs-Spheroids

To investigate the localization of CTL in spheroids, CTLc-spheroids and CTLs-spheroids were prepared as reported in Section 2.2, using a mixture of CTL and fluorescent-

labeled CTL (ratio 1:1). The spheroids were collected on day 4 and fixed in formaldehyde 4% *v*/*v* in PBS for 20 min at RT, following incubation in Triton-X100 0.2% in PBS for 15 min at RT. The samples were incubated with DAPI (1:1000 in PBS) for 10 min at RT to visualize cell nuclei, and then mounted on a microscope slide with Mowiol.

2.7. Immunohistochemistry of Integrins and Cadherins on Spheroids

Spheroids were collected and fixed in formaldehyde 4% *v*/*v* in PBS for 20 min at RT and incubated with Triton-X100 0.2% *v*/*v* in PBS for 15 min. Blocking solution (bovine serum albumin—BSA 4% *w*/*v*, normal goat serum—NGS 5% *v*/*v* in PBS) was added to spheroids and incubation was allowed for 1 h at RT. The primary antibodies were diluted in blocking buffer (integrin β1 antibody 1:200, E-cadherin antibody 1:300) and incubated with the spheroids at 4 °C overnight. The samples were then incubated for 2 h at RT with the secondary antibodies diluted in blocking buffer at the following concentrations: CruzFluor™ 647 for anti-integrin β1 antibody diluted 1:250; goat anti-rat Alexa Fluor™ 568 diluted 1:1000 for anti-E-cadherin antibody. DAPI was used to counterstain cell nuclei. The samples were mounted on a microscope slide using Mowiol and visualized by confocal microscopy using a Nikon C1si confocal microscope (Nikon, Tokyo, Japan), using a 40× Plan Apo objective (Nikon, Tokyo, Japan).

2.8. Real-Time PCR

CTLc-spheroids, CTLs-spheroids, and MF-spheroids were cultured in chondrogenic medium as described in Section 2.2. For the analysis of gene expression, total RNA was extracted by incubation in a phenol/chloroform mixture [13,16], transcribed in cDNA, and employed for qPCR analyses. Spheroids were collected by centrifugation (100× *g* for 5 min) on days 4 and 7, washed with PBS, and incubated with TRI-reagent (1 mL). Total RNA was purified according to the manufacturer's protocol. For cDNA synthesis, RNA (500 ng) from each sample was retrotranscribed with M-MLV reverse transcriptase and hexameric random primers. Gene expression levels of genes of interest were determined by quantitative real-time PCR (qPCR) using a CFX96 Real-Time PCR detection system (Bio-Rad Laboratories, Redmond, WA, USA) and SYBR Green methodology (Bio-Rad Laboratories, Redmond, WA, USA). The primer pair used to analyze gene expression levels (5′ to 3′) were as follows:

GAPDH_FW TCAAGGCTGAGAACGGGAAG
GAPDH_REV CGCCCCACTTGATTTTGGAG
COL2A1_FW CCTGGCAAAGATGGTGAGACAG
COL2A1_REV CCTGGTTTTCCACCTTCACCTG

The expression of the housekeeping gene GAPDH was used to normalize target gene expression, and the relative expression levels were calculated using the $2^{-\Delta\Delta CT}$ method [17]. The results are representative of two independent experiments in triplicate. Statistical significance was calculated by unpaired *t*-test analysis. Values are presented as mean and error bars indicate standard errors (SEs).

2.9. Light Microscopy Analyses on Spheroids

Spheroids were cultured in chondrogenic medium as described in Section 2.2 and collected on days 4 and 6 for light microscopy analyses. The samples were washed with PBS and fixed with paraformaldehyde (4% *w*/*v* in PBS) for 20 min at RT, washed again in PBS, and included in 100 µL of agarose gel (1.5% *w*/*v* in PBS). After two brief washings in PBS, the samples underwent dehydration through the ascending series of alcohols; the samples were kept for 2 h in each alcohol solution (50%, 70%, 96%, and absolute alcohol (*v*/*v*)), followed by two passages of 1 h each in xylene to clarify them before finally being embedded in paraffin. Following this, the samples were cut using a manual rotary Leitz

1512 microtome into sections with a thickness of 4 µm. The slices were then de-waxed (xylene and alcohol at progressively lower concentrations) and underwent hematoxylin–eosin (H&E) and Masson's Trichrome staining. For H&E staining (Bio-Optica, Milan, Italy), the slides were incubated for 15 min in the presence of hematoxylin followed by 7 min in eosin, dehydrated, and mounted with xylene-based balsam. Masson's Trichrome staining (Bio-Optica, Milan, Italy) was performed following the manufacturer's instructions. For each experimental point, images of stained sections were randomly selected and acquired using a Leica DM 4000 light microscope (Leica Cambridge Ltd., Cambridge, UK) with a Leica DFC 320 camera (Leica Cambridge Ltd., Cambridge, UK). Image acquisition was carried out with Leica Application Suite X (LASX) (Leica Cambridge Ltd., Cambridge, UK) image analysis software (version 3).

2.10. Transmission Electron Microscopy (TEM) on Spheroids

Spheroids were cultured in chondrogenic medium as described in Section 2.2 and collected on days 4 and 6 for TEM analyses. The samples were washed in PBS and fixed with glutaraldehyde 2.5% (*v*/*v*) in phosphate buffer 100 mM, pH 7.4, for 2.5 h at 4 °C. The samples were washes three times in 150 mM cacodylate buffer, post-fixed in OsO4 1% (*v*/*v*) in 100 mM cacodylate buffer for 30 min at RT, washed in 150 mM cacodylate buffer, dehydrated with acetone solutions of increasing concentration (50%, 70%, 80%, 90%, and 100% *v*/*v*), and embedded in epoxy resin starting from absolute acetone and epoxy resin (ratio 1:1) for 2 h at room temperature, followed by incubation in a solution of absolute acetone and epoxy resin (ratio 1:3) overnight at RT. Then, the samples were left in absolute epoxy resin for 7 h and incubated for two days at 60 °C to complete the embedding procedure. Ultrathin sections of 100 nm were cut using a Diatome diamond knife (Diatome, Hatfield, PA, USA) on a Reichert Jung ultracut E ultramicrotome (Reichert-Jung，Leica Microsystems GmbH, Wetzlar, Germany). Sections were picked up on nickel grids and stained by uranyl acetate solution and lead citrate, and then observed by a transmission electron microscope (CM10 Philips, FEI Company, Eindhoven, The Netherlands) at an accelerating voltage of 80 kV. Images were recorded by a Megaview III digital camera (FEI Company, Eindhoven, The Netherlands).

3. Results

3.1. The Involvement of Integrins and Cadherins in the Dynamics of CTL-Spheroid and MF-Spheroid Formation

To investigate the role of integrins and cadherins in spheroid formation and their interactions with the polysaccharide, CTLc-spheroids were grown in the presence of blocking antibodies selective for E-cadherin, β1-, and β3-integrins. MF-spheroids were employed as a control. The effect of these blocking molecules was investigated after 5 and 24 h of treatment (Figure 1).

In the case of MF-spheroids, compared to the untreated samples (Figure 1a,b), the effect of cadherin inhibition has little impact at 5 h, while it becomes more evident at 24 h (Figure 1e,f). At this time point, the cellular aggregates display reduced dimensions and compactness with a higher number of single, non-associated cells. The analysis of the effect of integrin blocking at 5 and 24 h reveals spheroids with morphology and shapes similar to the control (Figure 1i,j).

Differently, in CTLc-spheroids, the blocking of both E-cadherin and of β1- and β3-integrins (Figure 1g,h,k,l) significantly affects the assembly and coalescence of spheroids at 5 and 24 h from cell seeding, since smaller spheroids can be detected compared to the untreated sample (Figure 1c,d). It is interesting to observe that, conversely to untreated CTLc-spheroids and spheroids treated with anti-cadherin antibody, at 5 h, the inhibition

of integrin binding activity is not characterized by a distribution of cells along ribbon structures that act as initial centers of the cell association layer; rather, they are uniformly distributed (Figure 1k).

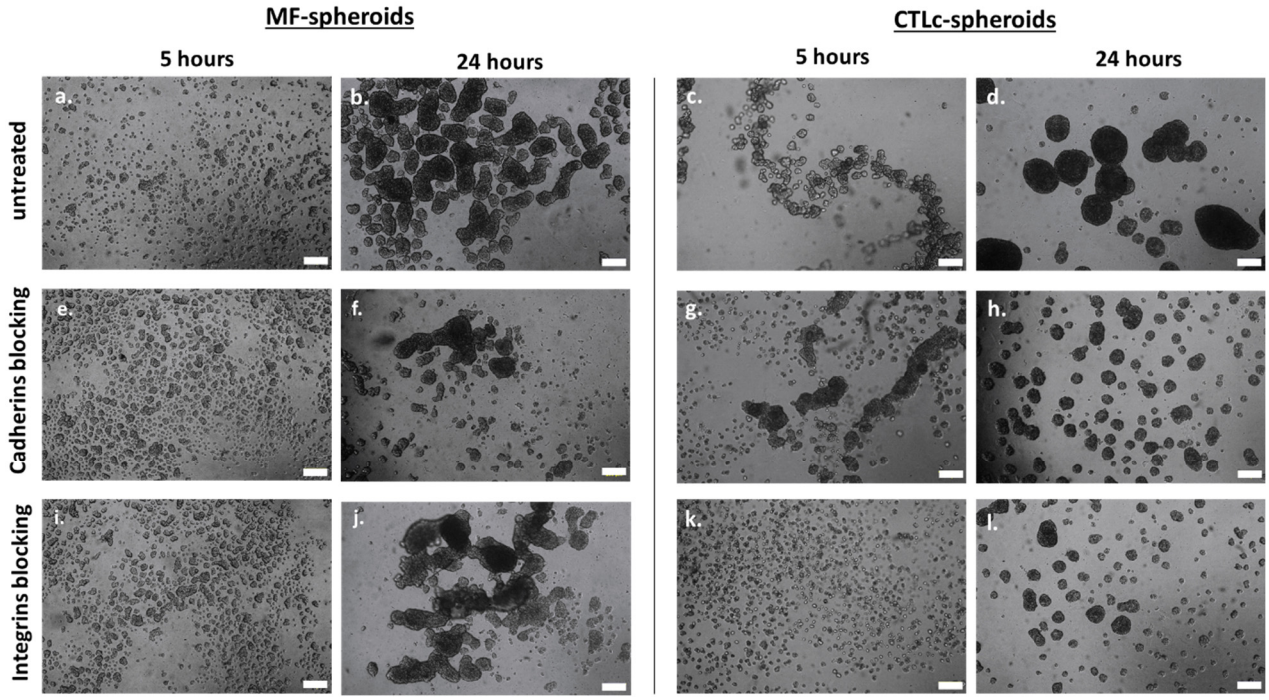

Figure 1. Optical images of MF- and CTLc-spheroids in the presence of integrin- and cadherin-blocking antibodies. The dynamics of spheroid formation in untreated MF-spheroids (**a**,**b**) and CTLc-spheroids (**c**,**d**) was compared to the dynamics of spheroid formation in the presence of anti-cadherin (**e**–**h**) and anti-integrin (**i**–**l**) antibodies, at 5 and 24 h from cell seeding (scale bar: 200 μm).

The involvement of cadherins and integrins in the dynamics and maturation of MF- and CTLc-spheroids was further investigated by immunohistochemical analyses on spheroids collected on days 4 and 6 (Figure 2). The samples were immunostained with E-cadherin and β1-integrin antibodies.

In MF-spheroids, integrin signal is only poorly detected on day 4 (Figure 2a,b); small integrin clusters, which are probably localized around clumps of newly produced ECM, can be observed only on day 6 (Figure 2c,d). On day 4, cadherin clusters can be observed (Figure 2e,f); the number and size of these clusters increases significantly by day 6, in parallel with the increasing compaction of the spheroids (Figure 2g,h).

In the case of the CTLc-spheroids, FITC-labeled polymer was employed to investigate the localization of the polymer with respect to that of proteins. Compared to MF-spheroids, on day 4, a higher expression of β1-integrin was observed (Figure 2i,j), which remained unchanged on day 6 (Figure 2k,l). In addition, it can be noticed that the protein clusters colocalize with the labeled polymer (white arrows in Figure 2l). On day 4, the cadherin signal appears similar to that recorded in MF-spheroids (Figure 2m,n), while on day 6, it appears lower (Figure 2o,p), although it could not be determined whether this was due to lower protein expression or to lower protein clustering.

3.2. Actin, Myosin, and Microtubules in the Process of Spheroid Formation

To investigate the role of the cytoskeleton in the dynamics of spheroid formation, MF- and CTLc-spheroids were treated with compounds capable of selectively inhibiting molecules involved in the dynamics of cytoskeletal rearrangements. The molecules employed were Cytochalasin D—CYT-D (inhibition of actin polymerization), ML-7 (inhibi-

tion of myosin light-chain kinase—MLCK), nocodazole (inhibition of microtubule polymerization), paclitaxel (inhibition of microtubule disassembly), and Y-27632 (inhibition of Rho-associated protein kinase—ROCK). These compounds were added to the cell culture medium immediately prior to cell seeding.

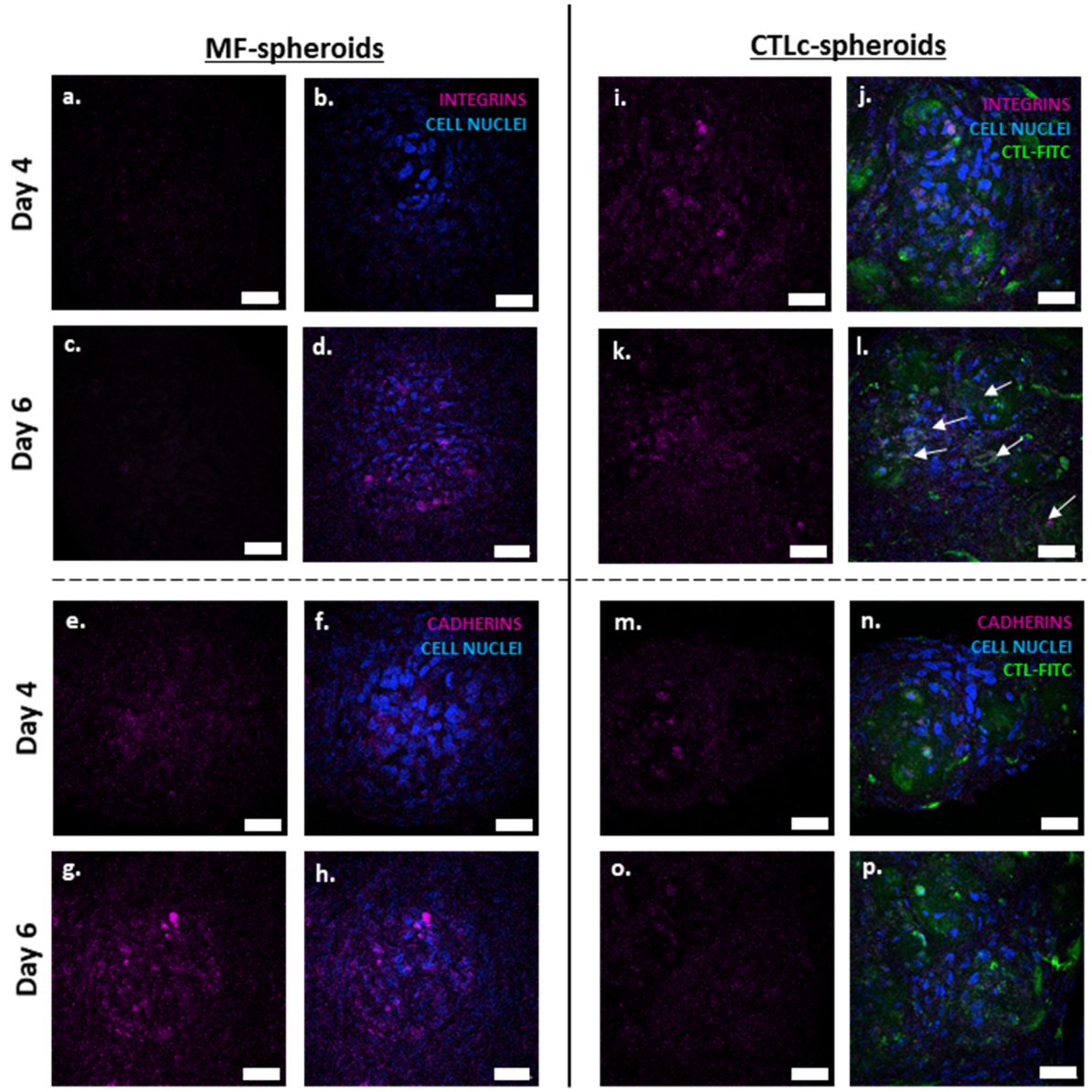

Figure 2. Immunohistochemical images of integrins and cadherins in MF- and CTLc-spheroids on days 4 and 6. Integrins (**a**–**d**,**i**–**l**) and cadherins (**e**–**h**,**m**–**p**) are stained in violet; cell nuclei are stained in blue (DAPI). In CTLc-spheroids, CTL-FITC is stained in green. White arrows indicate overlaps between CTL-FITC and protein clusters (scale bar: 50 μm).

In MF-spheroids, compared to untreated samples (Figure 3a,b), the inhibition of actin polymerization by CYT-D caused a complete impairment of cellular aggregation (Figure 3c,d). While initially no cell–cell interactions could be observed and cells appeared as single units, after 24 h, the cells formed a two-dimensional layer, but were unable to aggregate into 3D cell clusters.

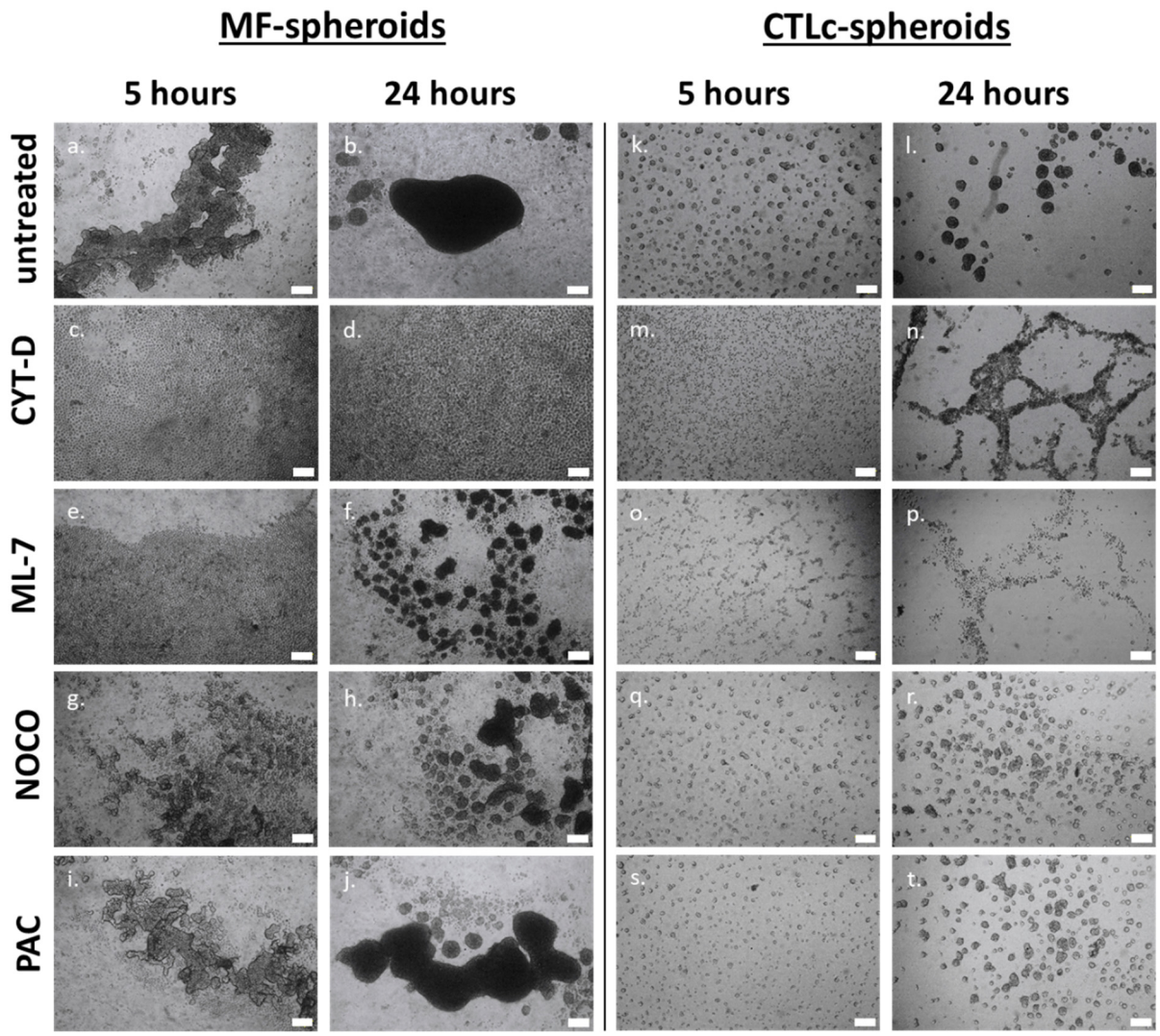

Figure 3. Optical images of MF- and CTLc-spheroids treated with compounds interfering with the dynamics of cytoskeletal rearrangements. The dynamics of spheroid formation in untreated MF-spheroids (**a**,**b**) and CTLc-spheroids (**k**,**l**) was compared to the dynamics of spheroid formation in the presence of Cytochalasin D—CYT-D (**c**,**d**,**m**,**n**), ML-7 (**e**,**f**,**o**,**p**), nocodazole—NOCO (**g**,**h**,**q**,**r**), and paclitaxel—PAC (**i**,**j**,**s**,**t**) at 5 and 24 h (scale bar: 200 μm).

A similar effect to CYT-D is achieved after 5 h of treatment with ML-7, as the cell–cell interaction is prevented (Figure 3e). However, the blocking of actomyosin contractility has a lower effect with longer incubation: compared to the control, at 24 h, MF-spheroids are formed, although they are smaller in size and less compact, with many interspersed free cells present (Figure 3f) [18]. In the presence of nocodazole, a slowing down of cell aggregation and coalescence is observed in MF-spheroids (Figure 3g,h), leading to the formation of smaller, irregularly shaped, less dense spheroids compared to the control. Differently, paclitaxel displays no significant influence on spheroid formation (Figure 3i,j). Finally, treatment with Y-27632 does not affect the dynamics of MF-spheroid formation (Figure S1a,b in Supporting Information). This suggests that, while in 2D cultures ROCK acts as a regulator of cytoskeletal rearrangements, the mechanism directing aggregation and spheroid formation does not specifically involve this signaling pathway [19].

In the presence of CTL, compared to untreated samples (Figure 3k,l), cell aggregation appears to be prevented by the treatment with CYT-D at 5 h (Figure 3m). After 24 h, the cells are distributed in a net-like pattern of loosely structured bunches. However, they

are unable to organize and compact into spheroidal structures and lead to coalescence phenomena (Figure 3n).

In the presence of ML-7, inhibitor of actomyosin contractility, the cells arrange in small groups characterized by weak cell interactions (Figure 3o), while at 24 h, loosely connected net-like cell aggregates appear (Figure 3p).

CTLc-spheroids seeded with either nocodazole (Figure 3q,r) or paclitaxel (Figure 3s,t) are smaller than the control group, both at 5 and 24 h after cell seeding. As for the treatment with Y-27632, no effects can be observed in CTLc-spheroids, suggesting that, as for MF-spheroids, the mechanism regulating the dynamics of spheroid formation does not specifically involve the ROCK signaling pathway (Figure S1c,d in Supporting Information).

3.3. Structural Features and Biological Response of Spheroids in Presence of CTL in Solution

As previously reported by Pizzolitto et al. [14] and Scognamiglio et al. [13], the CTL coating combines the inhibition of cell adhesion and the promotion of spheroid formation, establishing itself as a structurally integral part of the cell agglomerate. However, it was not clear how the physical transition from a dry coating to a rehydrated system occurs and to what extent the physicochemical nature of the polymer correlates with the biological response achieved, in terms of accelerating the expression of COL-2. To investigate the transition of CTL from an air-dried form to a rehydrated one, polysaccharide release studies were performed using FITC-labeled CTL. The data show that the fluorescent polymer is gradually released in the cell medium: after 5 h, 80% of the fluorescent polymer is detected, while from this point up to 24 h, a plateau is reached (Figure S2a in Supporting Information). DLS measurements, performed at the same time points (Figure S2b in Supporting Information), show that the signal of the rehydrated polymer coating is comparable to that of a CTL-containing solution, suggesting that the physical state is the same for the two samples (i.e., CTL in solution and rehydrated CTL coating).

CTL-spheroids were prepared by seeding the cells on agar gels in chondrogenic medium containing CTL in solution, hereafter referred to as CTLs-spheroids. The features and biological responses of CTLs-spheroids were investigated and compared to those of CTLc- and MF-spheroids. The kinetics of spheroid formation are reported in Figure 4a–f. The dimensional analysis demonstrates that CTLc- and CTLs-spheroids have a comparable average size and distribution on day 4 and both significantly differ from MF-spheroids (Figure 4g).

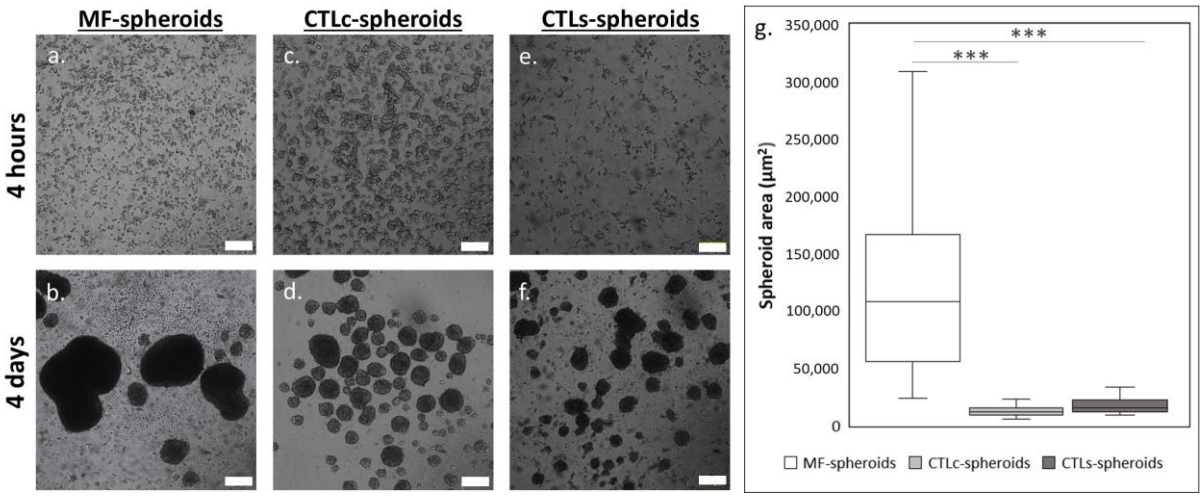

Figure 4. Optical images of MF-spheroids (**a**,**b**), CTLc-spheroids (**c**,**d**), and CTLs-spheroids (**e**,**f**) at 5 h and 4 days (scale bar: 200 μm). Dimensional distribution of spheroids on day 4 (**g**); (*** = p-value < 0.001).

By seeding cells in the presence of fluorescently labeled CTL, confocal visualization revealed that in CTLs-spheroids, the polymer is incorporated into spheroids (Figure 5c,d) and the cells are organized as concentric layers around CTL-FITC domains, resembling the distribution of the polysaccharide in CTLc-spheroids (Figure 5a,b). It can be assumed that in both systems, the cells bind to CTL, leading to the formation of hybrid polymer–cell spheroids in which the polymer is embedded.

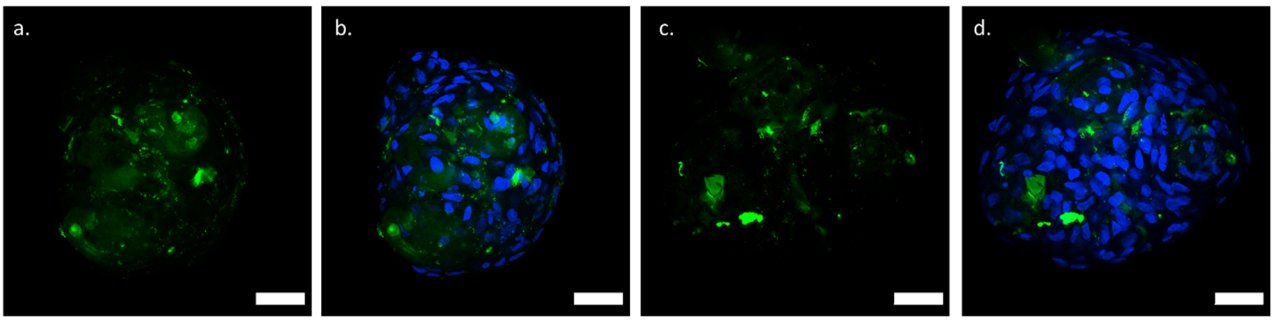

Figure 5. Localization of CTL-FITC in CTLc-spheroids (**a**,**b**) and CTLs-spheroids (**c**,**d**) on day 4. CTL-FITC is stained in green; cell nuclei are stained in blue with DAPI (scale bar: 50 µm).

Histological analysis was performed using hematoxylin–eosin and Masson's Trichrome staining on both CTLc- and CTLs-spheroids. In CTLc-spheroids on days 4 and 6, cells are detected mainly on the border of the structure rather than in the core (Figure 6a,b). Conversely, the core of the spheroid appears to be filled by an amorphous matrix, probably consisting of CTL (due to its ability to bind the dye), as the authors already reported in a previous paper [13]. The histological analysis performed on day 4 on CTLs-spheroids shows evidence of an organized inner architecture with viable cells and a compact ECM (Figure 6c). On day 6, in the CTLs-spheroids, a compact structure can be identified, along with close contact between the cells and the ECM. A good architecture with viable cells is preserved, despite these spheroids appearing bigger than those on day 4 (Figure 6d). Moreover, differently from CTLc-spheroids, cell distribution is detectable both on the edges and in the core. In both CTLc- and CTLs-spheroids, cell arrangement seems to reproduce chondroblast/osteoblast lacunae. Masson's Trichrome staining identifies collagen fibers in blue. An early deposition of collagen-based ECM can be recorded after 4 days of culture both in CTLc- and in CTLs-spheroids (Figure 6e,g) and the stain still appears detectable on day 6 (Figure 6f,h).

However, in CTLc-spheroids on day 4, a pale blue color identifies the weak presence of collagen (Figure 6e), whereas a consistent and discrete quantity of collagen fibers, well distributed both in the core and on the border of the spheroids, is noticeable in the CTLs-spheroids (Figure 6g). This deposition is maintained abundantly in CTLs-spheroids on day 6, with the blue staining becoming even more intense in smaller spheroids (Figure 6h), while for bigger spheroids, a reduction in both the blue staining intensity and collagen quantity can be observed.

The MF-spheroids appear larger than the CTLc- and CTLs-spheroids after 4 and 6 days of culture, and a structural analysis underlines the absence of chondrogenic/osteogenic lacunae (Figure S3a,b in Supporting Information). In the MF-spheroids on day 4, Masson's Trichrome staining highlights the lack of collagen fibers (Figure S3c in Supporting Information), while, after 6 days of culture, a very weak staining (pale blue) is observable, indicating a negligible ECM deposition compared with that recorded in the presence of CTLc- and CTLs-spheroids (Figure S3d in Supporting Information).

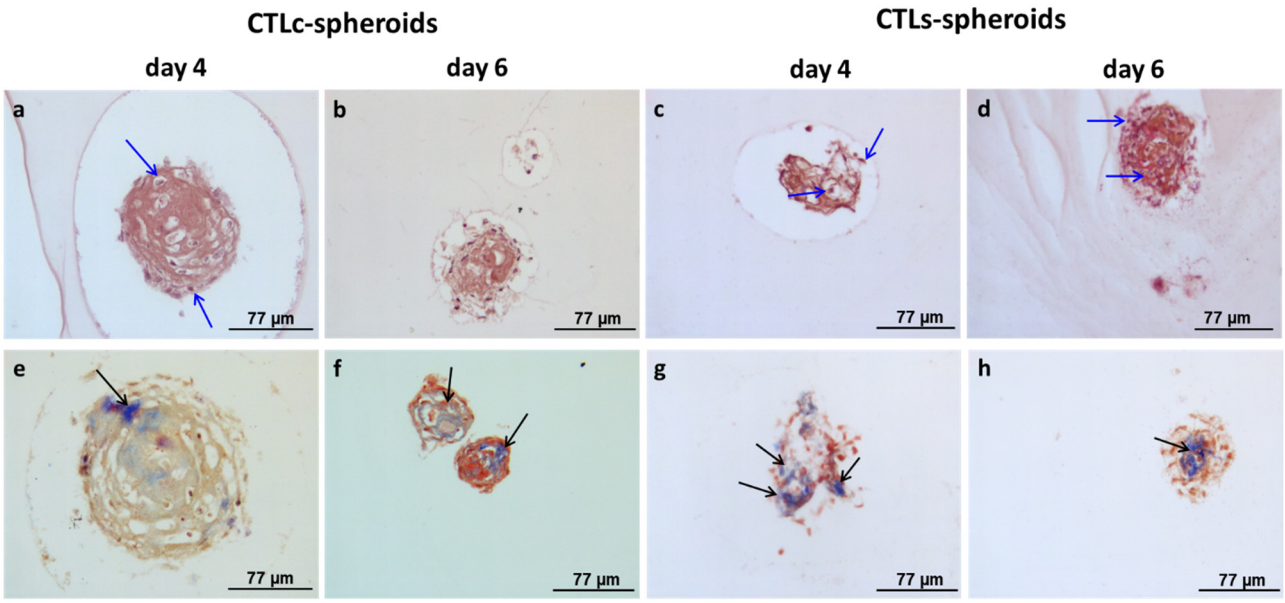

Figure 6. Hematoxylin–eosin staining (**a**–**d**) and Masson's Trichrome staining (**e**–**h**) on CTLc-spheroids and CTLs-spheroids on day 4 and day 6. Collagen appears as blue domains inside spheroids (scale bar 77 µm; magnification: 40×). Blue arrows indicate viable cells; black arrows indicate collagen, which appears as blue domains inside spheroids.

In both types of CTL-spheroids cultured for 4 days, TEM analyses showed cells with a polygonal shape (Figure 7a,e). At higher magnification, no mature collagenic fibers were detected in the ECM, while several thin filaments, possibly corresponding to precursor collagenic fibers, and a network structure most likely linked to CTL were identified (Figure 7b,f). By day 6, the cells are rich in vacuoles, autophagic vesicles, and rough endoplasmic reticulum (RER), with cell nuclei and nucleoli being easily detectable (Figure 7c,g). No signs of cellular distress attributable to apoptosis and/or necrosis can be observed. The cells are widely surrounded by ECM rich in the presence of banded collagen fibers (Figure 7d,h), suggesting the maturation of the previously synthetized protein. At higher magnification, collagen fibers can be seen tightly arranged around islets of amorphous material attributable to the polysaccharide chains of CTL (Figure 7d). CTL and the newly deposited matrix do not mix homogeneously, but tend to remain as separate entities.

MF-spheroids differ morphologically and structurally from those formed in the presence of CTL. They show a lower degree of mature collagen matrix synthesis, as already reported [13]. On day 4, the cells in MF-spheroids showed polygonal and irregular-shaped morphology with small and large intracytoplasmic vesicles (Figure S4a in Supporting Information). The extracellular matrix, although characterized by the presence of secreted components, did not show any mature fibrillar structure within it (Figure S4b in Supporting Information). After 6 days of chondrogenic differentiation, MF-spheroids still showed polygonal cells surrounded by extracellular matrix (Figure S4c in Supporting Information) characterized by the lack of mature organized fibrils (Figure S4d in Supporting Information).

COL2A1 gene expression was investigated by qRT-PCR (Figure 7i) in CTLc-, CTLs-, and MF-spheroids. The results are shown in Figure 7i, in which the gene expression of the samples with CTL was normalized against the gene expression in MF-spheroids at the same time point. Both cell systems with CTL show a remarkable increase in type II collagen (COL2A1) gene expression compared to control spheroids as early as day 4 of culture (~2000-fold for CTLc-spheroids and 2500-fold for CTLs-spheroids compared to

control spheroids). These results show a comparable expression pattern over time in both culture systems with CTL, albeit with different relative expression levels at each time point.

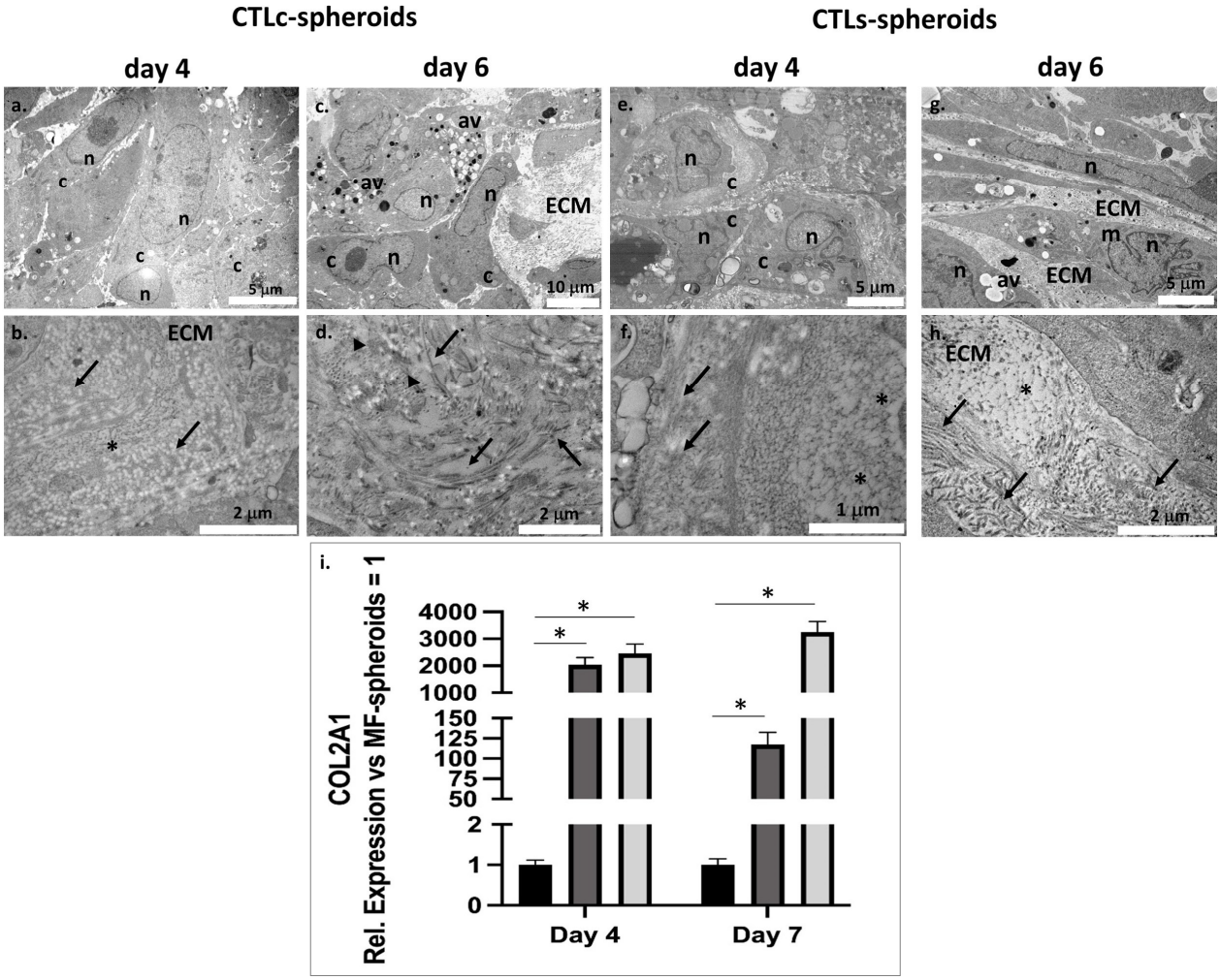

Figure 7. TEM images of CTLc- and CTLs-spheroids on day 4 and day 6 (**a**–**h**) and COL-2 gene expression by qPCR (**i**). In CTLc-spheroids on day 4, the cells show a polygonal shape, with a visible nucleus (n) and cytoplasm (c) (**a**). Details of ECM showing the presence of procollagen protein (black arrow) and CTL polymer (*) is reported (**b**). On day 6, MSCs in CTLc-spheroids show a polygonal and spindle shape. Lysosomes and autophagic vesicles (av) appear in the cytoplasm (**c**). The nucleus (n), mitochondria (m), and extracellular matrix (ECM) are visible (**c**). Details of ECM showing collagen fibers both in parallel (arrows) and transversal orientation (arrowheads) are reported (**d**). In CTLs-spheroids on day 4, the cells show a polygonal shape. Nucleus (n) and cytoplasm (**c**) can be detected (**e**). Details of extracellular matrix (ECM) showing the presence of procollagen protein (arrow) and CTL material (*) (**f**). In CTLs-spheroids on day 6, the cells showed a polygonal and spindle shape with nucleus (n), mitochondria (m), and extracellular matrix (ECM) visible. Lysosomes and autophagic vesicles (av) are detected in the cytoplasm (**g**). Details of extracellular matrix (ECM) showing collagen fibers in parallel and transversal orientation (arrows) and CTL (*) (**h**). Scale bar: (**a**): 5 µm; (**b**): 2 µm; (**c**): 10 µm; (**d**): 2 µm; (**e**): 5 µm; (**f**): 1 µm; (**g**): 5 µm; (**h**): 2 µm. Gene expression analysis shows that the expression of COL2A1 is anticipated in CTLc- and CTLs-spheroids compared to MF-spheroids. Data were normalized to the housekeeping gene GAPDH, and the relative expression of each gene was calibrated to that of MF-spheroids for each time point (set as 1). Data are presented as mean ± SE (black bars: MF-spheroids; dark gray bars: CTLc-spheroids; light gray bars: CTLs-spheroids) (**i**). (* = p-value < 0.05; unpaired t-test analysis).

4. Discussion

The dynamics of spheroid formation is based on the cross-action of adhesion molecules and cytoskeletal proteins, as cell aggregation and compaction are guided by molecular interactions and cellular rearrangements. The main cellular components involved in these phenomena are integrins and cadherins, respectively mediating cell adhesion to the ECM and to other cells, and the actin cytoskeleton [20]. Previous studies in which spheroids were produced on CTL coating (CTLc-spheroids) show that the kinetics of spheroid formation is delayed in the presence of CTL compared to spheroids without a matrix [13], suggesting the involvement of CTL as an active player in the dynamics of spheroid formation.

The results reported in Figure 1 demonstrate the different impact of integrins and cadherins in the dynamics of spheroid formation and highlight the interplay between these adhesion molecules and CTL. In MF-spheroids, cell aggregation primarily relies on cadherin-mediated interactions, which are involved in the early formation, growth, and coalescence of cell aggregates, while little contribution is given by integrins (Figure 1). In line with this observation, E-cadherin clusters can be detected already by day 4 with an increase in signal on day 6 (Figure 2). These adhesion molecules localize at the edge of cell–cell contacts, and their progressive signal increase is in line with the gradually surging compaction and coalescence of spheroids. Cadherins are known to control the fate of MSCs at early stages, by transducing biochemical signals from the microenvironment via the cadherin/catenin/actin cytoskeleton pathway, even impacting the progression of cell differentiation [21,22]. In pellet cultures, E-cadherin is critical in the condensation of initial cell aggregate [23], and the synergistic modulation of E- and N-cadherins was recently observed to enhance chondrogenesis [24]. In the later stages of chondrogenesis, MSCs experience a transition towards a microenvironment in which ECM interactions dominate. During this phase, there is an extensive crosstalk between signaling pathways activated by growth factor receptors and integrins binding to ECM components [21,22]. Cells in MF-spheroids appear to follow this molecular dynamic, which has also been observed in vivo. In fact, MF-spheroids show small integrin clusters only on day 7, likely localized around clumps of newly produced ECM (Figure 2). In the presence of CTL, the blocking of both cadherins and integrins affects spheroid formation, as smaller spheroids form over time compared to the control (Figure 1). The achievement of lower dimensions suggests that, in the presence of CTL, both integrins and cadherins are fundamental not only for the aggregation of cells, but also for the growth and coalescence of the aggregates. From this perspective, immunohistochemical analyses on CTLc-spheroids shows evidence of the presence of integrin clusters surrounding polymer clumps, and the extent of cadherin clusterization is lower than that observed in MF-spheroids (Figure 2). This suggests the existence of an interplay between cells and the polymer mediated by these adhesion molecules. It is conceivable that in the presence of a molecule that mimics the ECM, the involvement of cadherins and integrins can be observed at earlier stages of cellular aggregation, mediating cell–cell and cell–ECM interactions. After cell seeding, the polymer is rehydrated and further released in cell medium, where it can coordinate and guide cell assembly. CTL provides a structural matrix that supports spheroid organization and cell anchoring via integrins. In CTLc-spheroids, an equilibrium between a reduced amount of E-cadherin polymerization, the earlier activation of β1- and β3-integrins, and CTL incorporation may account for the dynamics of cell association and spheroid coalescence.

Cadherins and integrins are intrinsically linked to the actin cytoskeleton and share common signaling molecules. As for cadherins, a key component of the adherent junctions is the cadherin–catenin adhesion complex, interacting with actin filaments through the myosin II motor for cytoskeletal rearrangement [25]. The involvement of the actin–myosin

cytoskeleton and of microtubules in the maturation and mechanoregulation of integrin-mediated focal adhesions has been described [26–28].

The results reported in Figure 3 indicate that actin polymerization has a primary role in MF-spheroid formation: actin inhibition defines actin's role in spheroid formation as a mediator of both cell aggregation and structural compaction, while the primary associative interactions are mediated mainly by cadherins. Indeed, the actin polymerization-dependent protrusive activity operates continuously to push lateral membranes of neighboring cells together to keep cadherins in contact, favoring cell junction maturation and promoting cell aggregation and structural compaction [29]. It is reasonable to assume that by inhibiting actin polymerization—and, therefore, in the absence of these pushing forces—MF-spheroid formation is prevented, as it lacks the physical contribution necessary to support cell clusterization following the initiation of cadherin-mediated cell–cell interactions. It can be speculated that in the absence of an external matrix, spheroid formation occurs through an actin polymerization-dependent mechanism upon the establishment of cadherin-mediated cell–cell interactions.

While actin polymerization is crucial for cell aggregation in MF-spheroids, myosin contractility influences both early cell aggregation and cluster compaction and coalescence. When MLCK is inhibited, cell aggregation is delayed, and the lagging cell clusters lack the ability to coalesce and achieve a high degree of cellular compactness. These results are consistent with the observation that cytoskeletal contractility mediated by myosin II allows the accumulation of cadherins at the cell–cell interface, thus producing adhesive ligation and favoring cell–cell cohesion and the compaction of the cell aggregates [30].

In 2D cell cultures, a direct crosstalk between actin fibers and microtubules governs cell–substrate interactions [31]. Moreover, microtubule assembly and disassembly influences cadherin-mediated cell–cell adhesion [32]. According to our results, the inhibition of microtubule disassembly by paclitaxel does not significantly affect MF-spheroid formation. Conversely, the inhibition of microtubule polymerization by nocodazole affects the kinetics of cell aggregation and spheroid coalescence, leading to the formation of smaller, irregularly shaped, and less dense spheroids compared to the control. The effect elicited by nocodazole is less pronounced than that achieved by molecules interfering with the actin–myosin system, suggesting that the latter is the main driving force in spheroid formation. Our data are consistent with what is reported in [20], showing that microtubule depolymerization slows down the aggregation and compaction of spheroid formation of different tumor and non-tumor cell lines.

In the presence of CTL, the dynamics of spheroid formation differ to those of MF-spheroids. The inhibition of actin polymerization appears to negatively affect cell–cell aggregation at early time points; at later stages, the cells are able to organize in net-like structures of loosely connected cells and that likely originate from the interactions of cells with CTL. These structures cannot coalesce to form spheroids. These net-like structures could be the result of the integration of loose forms of cell–cell association mediated by cadherins and cell–polymer interactions mediated by integrins. This result suggests that actin polymerization accounts for the efficiency of cell–cell aggregation and for the subsequent phase of spheroid coalescence in CTLc-spheroids as well. However, differently from cadherin-mediated interactions, which affect the early stages of MF-spheroid formation, integrin-mediated interactions do not immediately require actin polymerization (Figure 3).

The effects caused by the reduction in actomyosin contractility have a different impact on spheroid formation depending on both the mechanism of compaction and cell type [33,34]. In CTLc-spheroids, inhibiting actomyosin contractility has a significant destabilizing effect on both cell–cell and cell–polymer interactions (Figure 3), affecting

the overall process of spheroid formation. These results indicate that the inhibition of myosin-mediated contractility destabilizes both cadherin-based aggregation and integrin-driven aggregation.

As for the contribution of microtubule assembly and disassembly in CTLc-spheroids, both of these processes seem to influence spheroid coalescence and growth. In this regard, the existence of a complex interplay among the microtubule cytoskeleton, the maturation state of the integrin-based focal adhesion complex, and the intracellular contractile force has been reported [26,35]. Since integrin–polymer interaction is supposed to be an important effector for the aggregation of CTLc-spheroids, treatment with cytoskeleton inhibitors could contribute to the delayed kinetics of spheroids by affecting the maturation of integrin-mediated adhesions.

Considering these data, it can be hypothesized that, in the presence of CTL, the dynamics of spheroid formation involves three main phases. In the first phase, integrin-mediated cell–polymer interactions are established, without requiring polymerized actin. This process is followed by a second phase, where cadherin-mediated cell–cell interactions predominate, and these interactions are stabilized by actin polymerization. The third phase is characterized by the progressive formation and strengthening of cadherin-based cell–cell junctions and integrin-based focal adhesions, with a densification of the spheroidal structures and further coalescence, which requires the polymerization of actin filaments. A summary of the role exerted by the different cellular components in the dynamics of MF- and CTLc-spheroids is reported in Figure 8a–d and Table 1.

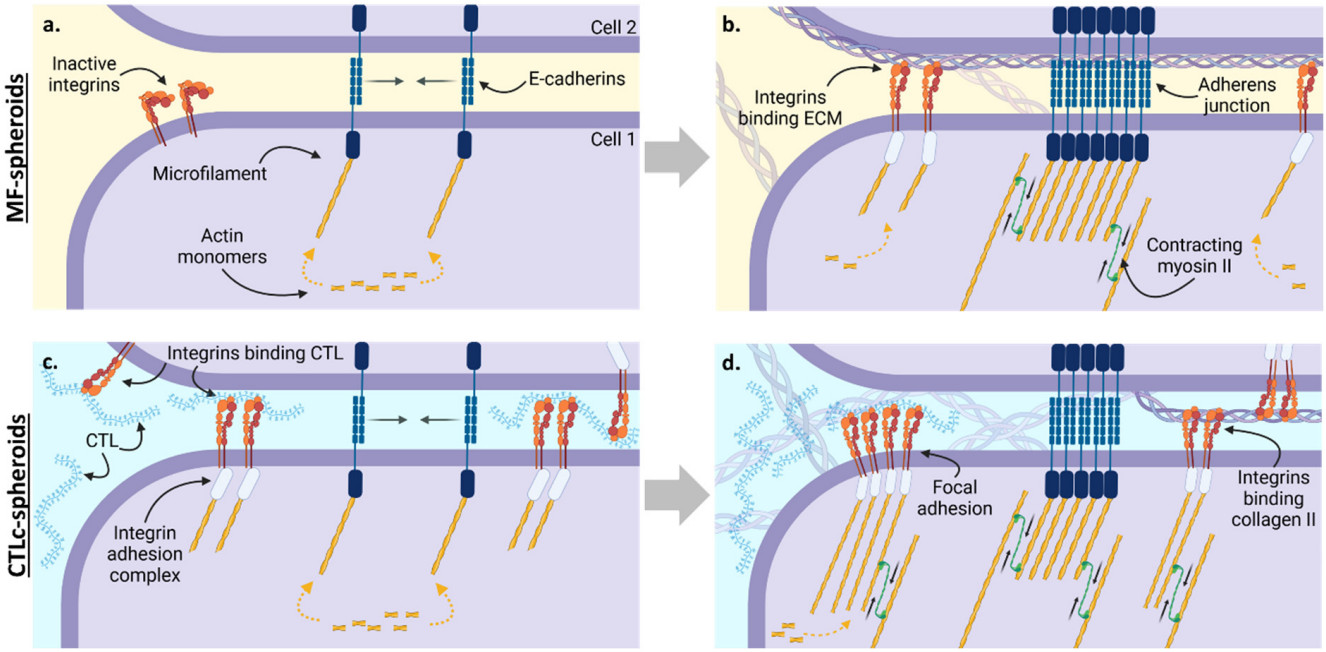

Figure 8. Dynamics of MF- and CTLc-spheroid formation. In MF-spheroids, cadherin homodimerization mediates initial cell aggregation, with integrins contributing little (**a**). As actin polymerizes and cadherins gradually cluster, actomyosin contraction further promotes junction maturation and spheroid compaction. Integrins contribute to spheroid growth only at a later stage, binding newly produced ECM (**b**). In CTLc-spheroids, integrins engage CTL from the earliest stages, promoting the formation of polymer-containing cell aggregates (**c**). Cadherin homodimerization progresses in a fashion similar to MF-spheroids, although CTL matrix allows for looser structure formation (**d**).

Table 1. Cellular components and biological mechanisms involved in the formation of MF-spheroids and CTLc-spheroids. Summary of key cellular components and their roles in spheroid formation. The involvement of E-cadherin, integrins, actin, MLCK, and microtubules is supported by experimental data from this study (Figures 1–3). The role of ROCK is included based on prior literature, as its function was not confirmed experimentally in this study.

	Biological Mechanism	**Role in MF-Spheroid Dynamics**	**Role in CTLc-spheroid Dynamics**
E-cadherin	Cell–cell interaction	Mediate cell–cell aggregation; primary role in early stages (Figures 1 and 2)	Mediate cell–cell aggregation and spheroid coalescence in early and late stages (Figures 1 and 2)
β1–β3 integrins	Cell–ECM interaction	Exert a minor role in spheroid formation (Figures 1 and 2)	Mediate cell–ECM aggregation and spheroid coalescence in early and late stages (Figures 1 and 2)
Actin fibers	Assembly and disassembly	Generate pushing forces on cadherins that allows cell aggregation and increase cell cohesion (Figure 3)	Generate pushing forces on cadherins that allows cell aggregation; No impact on integrin-binding activity (Figure 3)
MLCK	Actomyosin contractility	Accumulation of cadherins at cell–cell interface which accounts for spheroid coalescence and compactness (Figure 3)	Progressive formation and strengthening of cell–cell interactions, with a densification of the spheroidal structures and further coalescence (Figure 3)
Microtubules	Assembly and disassembly	Microtubule depolymerization holds a minor role in the regulation of spheroid coalescence (Figure 3)	Microtubule dynamics participate in spheroid coalescence (Figure 3)
ROCK	Myosin light chain phosphorylation	----	--

Morphological and molecular analyses show that the cells are able to interact with the polymer both as dry coating and when in solution. The two culture systems, one in the presence of a polymer coating and the other in the presence of a polymer solution, show comparable and overlapping biological responses, which are mainly characterized by increased differentiation capacity within a short timeframe. The morphological analysis of the CTLs- and CTLc-spheroids showed the deposition of collagenic extracellular matrix for both systems only after 4 days of differentiation (Figures 6 and 7). An ultrastructural analysis using TEM highlighted the presence of a highly developed RER and lysosomes, morphological features consistent with a chondrogenic phenotype [36]. The presence of mature collagen fibers was clearly detected on day 6. These observations are also supported by qRT-PCR data, highlighting that both CTL-spheroids have a similar early induction of COL2A1 expression. COL2A1 mRNA and matrix deposition were localized on day 4, while the newly synthetized matrix, visible in TEM images due to its characteristic banding, was processed into mature collagen on day 6. The peculiar organization of the cells and polysaccharide matrix in spheroids leads to the hypothesis that the polymer provides an architecture that promotes differentiation through both biochemical and mechanical signals.

Although chondrogenic differentiation in MSCs traditionally follows a TGF-β-mediated pathway over approximately 21 days, alternative pathways may be activated in the presence of mechanical cues. In the literature, the role of integrin-mediated signaling in MSC chondrogenesis, particularly under mechanical stimuli, is supported [37–40].

In particular, since qPCR data indicate an earlier expression of the COL2A1 gene in CTL-spheroids, it is conceivable that mechanical interactions between cells and the CTL matrix contribute to this upregulation [41,42]. Such mechanical stimuli may promote integrin-mediated receptor interactions that, together with TGF-β signaling, could facilitate an earlier induction of COL2A1 expression. Importantly, our observation that MF- and CTL-spheroids exhibit similar COL2A1 levels in the absence of TGF-β suggests that TGF-β plays an essential role in this process. While other factors might also contribute to this effect, these findings suggest a role for integrin-mediated mechanotransduction in the early upregulation of COL2A1. Indeed, the specific chemical structure of CTL, particularly the presence of lactitol side chains, could influence cell adhesion and differentiation through biochemical interactions beyond purely mechanical signaling. To this end, future studies will quantify this modulation of chondrogenic differentiation by screening both mechanical properties and biochemical cues of CTL.

5. Conclusions

During CTL-spheroid formation and development, the polymer influences the dynamics of cell adhesion molecule activation and cytoskeletal reorganization. From this perspective, CTL might provide a structural matrix for early integrin-mediated cell anchoring immediately after cell seeding. In this case, with both integrins and cadherins driving early CTL-spheroid formation, actin–myosin contractility and stress fiber polymerization simultaneously contribute to the spatial reorganization of cells, forming structures that are fundamentally different from their MF counterparts. Afterwards, the specific crosstalk between actin and microtubule cytoskeletal components regulates spheroid growth in both CTL- and MF-spheroids through the coalescence of cell aggregates. Compared to MF-spheroids, CTL-spheroids exhibit earlier COL2A1 gene expression and increased matrix deposition and maturation, suggesting an influence on the timing of differentiation. Furthermore, both physical forms of CTL studied in this work appear to significantly stimulate chondrogenicity, suggesting that the effect of the molecule is not dependent on its physical form, but rather on biochemical factors. Future studies will investigate the underlying molecular mechanisms and pathways responsible for this accelerated chondrogenesis, comparing CTL's effects with other polysaccharide-based systems. This mechanistic understanding is a critical prerequisite for future in vivo studies, representing a potential next step in assessing CTL's therapeutic potential for cartilage regeneration.

Supplementary Materials: The following supporting information can be downloaded at: https://www.mdpi.com/article/10.3390/polysaccharides6020047/s1, Figure S1. MF-spheroids (a,b) and CTLc-spheroids (c,d) treated with Y-27 for 5 and 24 h. Figure S2. Release of CTL-FITC after rehydration of CTL-coating (a); dynamic light scattering (DLS) analysis of CTL solution and rehydrated CTL-coating (b). Figure S3. Hematoxylin-eosin staining (a,b) and Masson's Trichrome staining (c,d) of MF-spheroids at days 4 and 6. Figure S4. TEM images of MF-spheroids at day 4 (a,b) and day 6 (c,d).

Author Contributions: Conceptualization: M.C., F.S., I.D., and E.M.; Investigation: M.C., F.S., S.Z., G.T., and M.R.; Supervision: E.M.; Writing—original draft: M.C., F.S., and E.M.; Writing—review and editing: I.D., S.Z., G.T., and M.R. All authors have read and agreed to the published version of the manuscript.

Funding: This research received no external funding.

Data Availability Statement: The original contributions presented in this study are included in the article/Supplementary Material. Further inquiries can be directed to the corresponding author(s).

Acknowledgments: Francesco Piazza (University of Trieste) is acknowledged for informatics support using GraphPad Prism version 10.4.2 for Windows, GraphPad Software, Boston, MA, USA, www.graphpad.com. Figure 8a–d and the Graphical Abstract were created in BioRender.com (Graphical Abstract: Created in BioRender. Donati, I. (2025) https://BioRender.com/t600hf5. Figure 8a: Created in BioRender. Conz, M. (2025) https://BioRender.com/ntb5r0z. Figure 8b: Created in BioRender. Conz, M. (2025) https://BioRender.com/8ytswvj. Figure 8c: Created in BioRender. Conz, M. (2025) https://BioRender.com/qfeclaq. Figure 8d: Created in BioRender. Conz, M. (2025) https://BioRender.com/nxe7iyf). All images were accessed on 28 March 2025.

Conflicts of Interest: The authors declare that they have no known competing financial interests or personal relationships that could have appeared to influence the work reported in this paper.

References

1. Chen, M.; Jiang, Z.; Zou, X.; You, X.; Cai, Z.; Huang, J. Advancements in Tissue Engineering for Articular Cartilage Regeneration. *Heliyon* **2024**, *10*, e25400. [CrossRef] [PubMed]
2. Li, M.; Yin, H.; Yan, Z.; Li, H.; Wu, J.; Wang, Y.; Wei, F.; Tian, G.; Ning, C.; Li, H.; et al. The Immune Microenvironment in Cartilage Injury and Repair. *Acta Biomater.* **2022**, *140*, 23–42. [CrossRef] [PubMed]
3. Casey, R.C.; Burleson, K.M.; Skubitz, K.M.; Pambuccian, S.E.; Oegema, T.R.; Ruff, L.E.; Skubitz, A.P.N. β1-Integrins Regulate the Formation and Adhesion of Ovarian Carcinoma Multicellular Spheroids. *Am. J. Pathol.* **2001**, *159*, 2071–2080. [CrossRef] [PubMed]
4. Lin, R.-Z.; Chou, L.-F.; Chien, C.-C.M.; Chang, H.-Y. Dynamic Analysis of Hepatoma Spheroid Formation: Roles of E-Cadherin and β1-Integrin. *Cell Tissue Res.* **2006**, *324*, 411–422. [CrossRef]
5. Pillai, V.V.; Koganti, P.P.; Kei, T.G.; Gurung, S.; Butler, W.R.; Selvaraj, V. Efficient Induction and Sustenance of Pluripotent Stem Cells from Bovine Somatic Cells. *Biol. Open* **2021**, *10*, bio058756. [CrossRef]
6. Yun, C.; Kim, S.H.; Kim, K.M.; Yang, M.H.; Byun, M.R.; Kim, J.-H.; Kwon, D.; Pham, H.T.M.; Kim, H.-S.; Kim, J.-H.; et al. Advantages of Using 3D Spheroid Culture Systems in Toxicological and Pharmacological Assessment for Osteogenesis Research. *Int. J. Mol. Sci.* **2024**, *25*, 2512. [CrossRef]
7. Ko, J.-Y.; Lee, E.; Park, J.-W.; Kim, J.; Im, G.-I. Enhancement of Cartilage Regeneration Efficiency with Human Adipose Stem Cell Three Dimensional Spheroid. *Osteoarthr. Cartil.* **2020**, *28*, S515–S516. [CrossRef]
8. Ahmad, T.; Lee, J.; Shin, Y.M.; Shin, H.J.; Madhurakat Perikamana, S.K.; Park, S.H.; Kim, S.W.; Shin, H. Hybrid-Spheroids Incorporating ECM like Engineered Fragmented Fibers Potentiate Stem Cell Function by Improved Cell/Cell and Cell/ECM Interactions. *Acta Biomater.* **2017**, *64*, 161–175. [CrossRef]
9. Gonzalez-Fernandez, T.; Tenorio, A.J.; Saiz, A.M., Jr.; Leach, J.K. Engineered Cell-Secreted Extracellular Matrix Modulates Cell Spheroid Mechanosensing and Amplifies Their Response to Inductive Cues for the Formation of Mineralized Tissues. *Adv. Healthc. Mater.* **2022**, *11*, 2102337. [CrossRef]
10. Scognamiglio, F.; Travan, A.; Borgogna, M.; Donati, I.; Marsich, E. Development of Biodegradable Membranes for the Delivery of a Bioactive Chitosan-Derivative on Cartilage Defects: A Preliminary Investigation. *J. Biomed. Mater. Res. A* **2020**, *108*, 1534–1545. [CrossRef]
11. Scognamiglio, F.; Travan, A.; Donati, I.; Borgogna, M.; Marsich, E. A Hydrogel System Based on a Lactose-Modified Chitosan for Viscosupplementation in Osteoarthritis. *Carbohydr. Polym.* **2020**, *248*, 116787. [CrossRef] [PubMed]
12. Pizzolitto, C.; Scognamiglio, F.; Sacco, P.; Lipari, S.; Romano, M.; Donati, I.; Marsich, E. Immediate Stress Dissipation in Dual Cross-Link Hydrogels Controls Osteogenic Commitment of Mesenchymal Stem Cells. *Carbohydr. Polym.* **2023**, *302*, 120369. [CrossRef] [PubMed]
13. Scognamiglio, F.; Pizzolitto, C.; Romano, M.; Teti, G.; Zara, S.; Conz, M.; Donati, I.; Porrelli, D.; Falconi, M.; Marsich, E. A Lactose-Modified Chitosan Accelerates Chondrogenic Differentiation in Mesenchymal Stem Cells Spheroids. *Biomater. Adv.* **2024**, *160*, 213849. [CrossRef] [PubMed]
14. Pizzolitto, C.; Scognamiglio, F.; Baldini, G.; Bortul, R.; Turco, G.; Donati, I.; Nicolin, V.; Marsich, E. Bioactive Lactose-Modified Chitosan Acts as a Temporary Extracellular Matrix for the Formation of Chondro-Aggregates. *ACS Appl. Polym. Mater.* **2023**, *5*, 504–516. [CrossRef]
15. Sacco, P.; Piazza, F.; Pizzolitto, C.; Baj, G.; Brun, F.; Marsich, E.; Donati, I. Regulation of Substrate Dissipation via Tunable Linear Elasticity Controls Cell Activity. *Adv. Funct. Mater.* **2022**, *32*, 2200309. [CrossRef]
16. Greco, S.; D'agostino, E.; Manfrin, C.; Gaetano, A.S.; Furlanis, G.; Capanni, F.; Santovito, G.; Edomi, P.; Giulianini, P.G.; Gerdol, M. RNA-Sequencing Indicates High Hemocyanin Expression as a Key Strategy for Cold Adaptation in the Antarctic Amphipod *Eusirus* Cf. *Giganteus Clade G3*. *BIOCELL* **2021**, *45*, 1611–1619. [CrossRef]

17. Livak, K.J.; Schmittgen, T.D. Analysis of Relative Gene Expression Data Using Real-Time Quantitative PCR and the $2^{-\Delta\Delta CT}$ Method. *Methods* **2001**, *25*, 402–408. [CrossRef]
18. Ernest, N.J.; Habela, C.W.; Sontheimer, H. Cytoplasmic Condensation Is Both Necessary and Sufficient to Induce Apoptotic Cell Death. *J. Cell Sci.* **2008**, *121*, 290–297. [CrossRef]
19. Amano, M.; Nakayama, M.; Kaibuchi, K. Rho-Kinase/ROCK: A Key Regulator of the Cytoskeleton and Cell Polarity. *Cytoskeleton* **2010**, *67*, 545–554. [CrossRef]
20. Smyrek, I.; Mathew, B.; Fischer, S.C.; Lissek, S.M.; Becker, S.; Stelzer, E.H.K. E-Cadherin, Actin, Microtubules and FAK Dominate Different Spheroid Formation Phases and Important Elements of Tissue Integrity. *Biol. Open* **2019**, *8*, bio037051. [CrossRef]
21. DeLise, A.M.; Fischer, L.; Tuan, R.S. Cellular Interactions and Signaling in Cartilage Development. *Osteoarthr. Cartil.* **2000**, *8*, 309–334. [CrossRef] [PubMed]
22. Song, E.K.; Park, T.J. Integrin Signaling in Cartilage Development. *Anim. Cells Syst.* **2014**, *18*, 365–371. [CrossRef]
23. Ryu, N.-E.; Lee, S.-H.; Park, H. Spheroid Culture System Methods and Applications for Mesenchymal Stem Cells. *Cells* **2019**, *8*, 1620. [CrossRef] [PubMed]
24. Tuli, R.; Tuli, S.; Nandi, S.; Huang, X.; Manner, P.A.; Hozack, W.J.; Danielson, K.G.; Hall, D.J.; Tuan, R.S. Transforming Growth Factor-β-Mediated Chondrogenesis of Human Mesenchymal Progenitor Cells Involves N-Cadherin and Mitogen-Activated Protein Kinase and Wnt Signaling Cross-Talk. *J. Biol. Chem.* **2003**, *278*, 41227–41236. [CrossRef]
25. Nelson, W.J. Regulation of Cell–Cell Adhesion by the Cadherin–Catenin Complex. *Biochem. Soc. Trans.* **2008**, *36 Pt 2*, 149–155. [CrossRef]
26. LaFlamme, S.E.; Mathew-Steiner, S.; Singh, N.; Colello-Borges, D.; Nieves, B. Integrin and Microtubule Crosstalk in the Regulation of Cellular Processes. *Cell. Mol. Life Sci.* **2018**, *75*, 4177–4185. [CrossRef]
27. Li, X.; Goult, B.T.; Ballestrem, C.; Zacharchenko, T. The Structural Basis of the Talin–KANK1 Interaction That Coordinates the Actin and Microtubule Cytoskeletons at Focal Adhesions. *Open Biol.* **2023**, *13*, 230058. [CrossRef]
28. Yu, M.; Le, S.; Ammon, Y.-C.; Goult, B.T.; Akhmanova, A.; Yan, J. Force-Dependent Regulation of Talin–KANK1 Complex at Focal Adhesions. *Nano Lett.* **2019**, *19*, 5982–5990. [CrossRef]
29. Li, J.X.H.; Tang, V.W.; Brieher, W.M. Actin Protrusions Push at Apical Junctions to Maintain E-Cadherin Adhesion. *Proc. Natl. Acad. Sci. USA* **2020**, *117*, 432–438. [CrossRef]
30. Maître, J.-L.; Heisenberg, C.-P. Three Functions of Cadherins in Cell Adhesion. *Curr. Biol.* **2013**, *23*, R626–R633. [CrossRef]
31. Rafiq, N.B.M.; Nishimura, Y.; Plotnikov, S.V.; Thiagarajan, V.; Zhang, Z.; Shi, S.; Natarajan, M.; Viasnoff, V.; Kanchanawong, P.; Jones, G.E.; et al. A Mechano-Signalling Network Linking Microtubules, Myosin IIA Filaments and Integrin-Based Adhesions. *Nat. Mater.* **2019**, *18*, 638–649. [CrossRef] [PubMed]
32. Gauthier-Rouvière, C.; Causeret, M.; Comunale, F.; Charrasse, S. Cadherin-Mediated Cell-Cell Adhesion and the Microtubule Network. In *Rise and Fall of Epithelial Phenotype: Concepts of Epithelial-Mesenchymal Transition*; Savagner, P., Ed.; Springer: Boston, MA, USA, 2005; pp. 288–296.
33. Devanny, A.J.; Vancura, M.B.; Kaufman, L.J. Exploiting Differential Effects of Actomyosin Contractility to Control Cell Sorting among Breast Cancer Cells. *Mol. Biol. Cell* **2021**, *32*, ar24. [CrossRef] [PubMed]
34. Napolitano, A.P.; Chai, P.; Dean, D.M.; Morgan, J.R. Dynamics of the Self-Assembly of Complex Cellular Aggregates on Micromolded Nonadhesive Hydrogels. *Tissue Eng.* **2007**, *13*, 2087–2094. [CrossRef] [PubMed]
35. Ng, D.H.J.; Humphries, J.D.; Byron, A.; Millon-Frémillon, A.; Humphries, M.J. Microtubule-Dependent Modulation of Adhesion Complex Composition. *PLoS ONE* **2014**, *9*, e115213. [CrossRef]
36. Francis, D.V.; Rajeswari, A.J.; Stephen, J.B.; Parasuraman, G.; Lisha, J.J.; Livingston, A.; Rani, S.; Daniel, A.J.; Sathishkumar, S.; Vinod, E. An Ultrastructural Report of Human Articular Cartilage Resident Cells in Correlation with Their Phenotypic Characteristics. *J. Histotechnol.* **2024**, *47*, 23–38. [CrossRef]
37. Goessler, U.; Bugert, P.; Bieback, K.; Stern-Straeter, J.; Bran, G.; Hörmann, K.; Riedel, F. Integrin Expression in Stem Cells from Bone Marrow and Adipose Tissue during Chondrogenic Differentiation. *Int. J. Mol. Med.* **2008**, *21*, 271–279. [CrossRef]
38. Wang, L.; Zheng, F.; Song, R.; Zhuang, L.; Yang, M.; Suo, J.; Li, L. Integrins in the Regulation of Mesenchymal Stem Cell Differentiation by Mechanical Signals. *Stem Cell Rev. Rep.* **2022**, *18*, 126–141. [CrossRef]
39. Zhang, T.; Wen, F.; Wu, Y.; Goh, G.S.H.; Ge, Z.; Tan, L.P.; Hui, J.H.P.; Yang, Z. Cross-Talk between TGF-Beta/SMAD and Integrin Signaling Pathways in Regulating Hypertrophy of Mesenchymal Stem Cell Chondrogenesis under Deferral Dynamic Compression. *Biomaterials* **2015**, *38*, 72–85. [CrossRef]
40. Mathieu, P.S.; Loboa, E.G. Cytoskeletal and Focal Adhesion Influences on Mesenchymal Stem Cell Shape, Mechanical Properties, and Differentiation down Osteogenic, Adipogenic, and Chondrogenic Pathways. *Tissue Eng. Part B Rev.* **2012**, *18*, 436–444. [CrossRef]

41. Kanazawa, T.; Furumatsu, T.; Hachioji, M.; Oohashi, T.; Ninomiya, Y.; Ozaki, T. Mechanical Stretch Enhances COL2A1 Expression on Chromatin by Inducing SOX9 Nuclear Translocalization in Inner Meniscus Cells. *J. Orthop. Res.* **2012**, *30*, 468–474. [CrossRef]
42. Chiquet, M.; Koch, M.; Matthisson, M.; Tannheimer, M.; Chiquet-Ehrismann, R. Regulation of Extracellular Matrix Synthesis by Mechanical Stress. *Biochem. Cell Biol.* **1996**, *74*, 737–744. [CrossRef]